Generating stable tractor beams with dielectric metasurfaces

Carl Pfeiffer and Anthony Grbic*

Department of Electrical Engineering and Computer Science, University of Michigan, Ann Arbor, Michigan 48109-2122, USA

(Received 26 November 2014; revised manuscript received 12 February 2015; published 6 March 2015)

Propagation-invariant beams that pull objects towards a light source are commonly known as tractor beams. Here, an efficient, linearly polarized tractor beam with improved stability is introduced. The beam consists of a superposition of transverse-electric and transverse-magnetic polarized Bessel beams of orders $m = +1$ and $m = -1$. It is shown that this beam can stably pull a wide range of dielectric microparticles arbitrarily long distances, independent of ambient conditions. Next, a straightforward method of generating these high-performance beams is proposed. A Si metasurface transforms an incident linearly polarized Gaussian beam into the desired tractor beam. Full-wave simulations demonstrate that it is possible for this simple geometry to pull a polystyrene sphere a distance equal to the nondiffracting range of the Bessel beam. The simplicity of the setup and the robust performance of the proposed tractor beam significantly enhance the ability to manipulate matter with light.

DOI: 10.1103/PhysRevB.91.115408 PACS number(s): 42.50.Wk, 37.10.Vz, 78.67.Pt

I. INTRODUCTION

Light can exert a force on matter, which has proven useful for a variety of applications such as manipulating and assembling nanostructures [1,2] or sorting bacteria and viruses [3–5]. Propagation-invariant beams are particularly well suited for simultaneously trapping and aligning many particles [6]. These beams usually exert a positive radiation pressure on an object, which pushes particles away from the source. However, it was recently shown that a net pulling force can be generated if the beam is sufficiently nonparaxial [7–9]. To date, many different methods of generating these so-called "tractor beams" have been proposed [10]. For example, optical solenoid beams have pulled silica microparticles distances of 8 μm [11]. Alternatively, simply interfering two Gaussian beams with each other can pull polystyrene microspheres distances exceeding 30 μm [12]. However, this particular method is inherently inefficient since Gaussian beams do not have a high-intensity focus. Therefore, the vast majority of light never actually interacts with the particle of interest. Many other methods of pulling particles towards a source using light [13], sound [14], or currents in fluids [15] have recently been proposed, but they require a strong interaction between the particle and the surrounding media. Optical conveyor belts can also move objects towards a light source over significant distances [16,17]. However, these beams actively move particles using tunable optical components, which is conceptually different than a passive tractor beam.

The goal here is to efficiently pull a wide range of particles towards a source, independent of ambient conditions. Propagation-invariant Bessel beams focus their energy towards the beam axis, which make them ideal for interacting with particles over large distances [6,8,9,18,19]. For a given incident power, Bessel beams can achieve pulling forces that are orders of magnitude larger than interfering Gaussian beams. In particular, first-order Bessel beams with both transverse-magnetic (TM) and transverse-electric (TE) polarizations provide the maximal pulling force. However, the pulling force imparted by these beams is sensitive to the particle's permittivity and size [20]. In addition, these beams require significant damping from the surrounding fluid (i.e., viscous drag) for stable on-axis transverse trapping [19,21]. These limitations have made the experimental demonstration of a Bessel-mode tractor beam elusive.

Here, it is analytically shown that a superposition of nondiffracting Bessel beams of orders $m = +1$ and $m = -1$ can stably pull dielectric particles over significant distances, in both damped and undamped conditions. This beam exerts an identical pulling force as previously reported first-order Bessel beams [9], but confines the particle near the beam axis. Next, it is shown that a tractor beam can be straightforwardly generated by illuminating a low-loss dielectric metasurface with a normally incident Gaussian beam, as shown in Fig. 1. Full wave simulations verify the metasurface design, and demonstrate that the tractor beam can pull a polystyrene particle over the beam's nondiffracting range. The simplicity of the setup should make experimental validation of the proposed tractor beam straightforward.

II. HIGHER-ORDER BESSEL BEAMS FOR REALIZING TRACTOR BEAMS

The electric and magnetic fields of an mth-order Bessel beam propagating in the $\hat{\mathbf{z}}$ direction can be written as [22]

$$\mathbf{E} = E_0 e^{i\beta k_0 z + im\phi - i\omega t} \times \left(-J_m(qk_0\rho)c_2\hat{\mathbf{z}} + \frac{1}{q}c_1(\hat{\mathbf{z}} \times \mathbf{b}) - \frac{\beta}{q}c_2\mathbf{b} \right), \quad (1)$$

$$\mathbf{H} = \frac{E_0}{\eta_0} e^{i\beta k_0 z + im\phi - i\omega t} \times \left(-J_m(qk_0\rho)c_1\hat{\mathbf{z}} - \frac{1}{q}c_2(\hat{\mathbf{z}} \times \mathbf{b}) - \frac{\beta}{q}c_1\mathbf{b} \right), \quad (2)$$

where $\mathbf{b} = iJ'_m(qk_0\rho)\hat{\boldsymbol{\rho}} - (m/qk_0\rho)J_m(qk_0\rho)\hat{\boldsymbol{\phi}}$, and $J_m(qk_0\rho)$ is the mth-order Bessel function of the first kind and $J'_m(qk_0\rho) = \frac{dJ_m}{d(qk_0\rho)}$. The coefficients β and q are the longitudinal and transverse wave numbers normalized to the free-space wave number k_0, which satisfy the separation relation $(qk_0)^2 + (\beta k_0)^2 = k_0^2$. The beam can be decomposed

*To whom correspondence should be addressed: agrbic@umich.edu

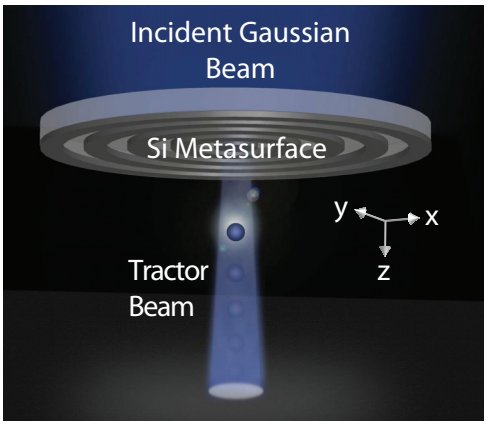

FIG. 1. (Color online) A Si metasurface converts a normally incident Gaussian beam into a tractor beam. The tractor beam pulls a dielectric particle up towards the source against the force of gravity.

into plane waves that exist on the surface of a cone with vertex angle $2\alpha = 2\sin^{-1}(q)$. The nonparaxiality of the beam is given by α. The beam contains both TE and TM polarizations, with complex amplitudes given by c_1 and c_2, respectively.

A. Circularly polarized tractor beam

To date, the Bessel beam with the strongest pulling force for a given incident power is a first-order Bessel beam with electric field $\mathbf{E}_1$ characterized by $m = 1, c_1 = 1$, and $c_2 = i$ [9,19–21]. This beam will be referred to as a circularly polarized tractor beam since the electric field is right-handed circularly polarized near the axis. In addition to the spin angular momentum provided by the circular polarization, this beam contains a net orbital angular momentum, which imparts a $\hat{\boldsymbol{\phi}}$-directed force on a particle near the beam axis [23]. This force is nonconservative since the work performed when moving a particle in a closed circle around the beam axis is nonzero. The circularly polarized beam continuously accelerates the angular speed of the particle, which drives it from the beam axis. Thus, the beam is unstable since it cannot trap particles in the transverse plane unless a significant frictional force (typically due to viscous drag) is also present [19].

B. Linearly polarized tractor beam

Let us consider adding another Bessel beam with opposite value of angular momentum (order $m = -1$) to the circularly polarized beam. This additional beam has an electric field denoted as $\mathbf{E}_{-1}$, and is characterized by coefficients $c_1 = 1$, and $c_2 = -i$, so it is left-handed circularly polarized near the beam axis. Intuitively, a superposition of $\mathbf{E}_1$ and $\mathbf{E}_{-1}$ can provide a stable pulling force since it contains no net orbital angular momentum. The addition of two circular polarizations of opposite handedness makes the beam linearly polarized near its axis

$$\lim_{k_0\rho\ll 1}(\mathbf{E}_1 + \mathbf{E}_{-1})/\sqrt{2} = \frac{E_0}{q\sqrt{2}}(\beta+1)\hat{\mathbf{x}}. \tag{3}$$

Therefore this beam will be referred to as a linearly polarized tractor beam.

III. OPTICAL FORCES EXERTED BY BESSEL BEAMS

In general, the force that light exerts on an object is characterized by a Maxwell stress tensor. When the object is subwavelength, it can be modeled as a combination of an electric and magnetic dipole, which simplifies the analysis [24]. The time-averaged force on a small particle can be written as

$$\mathbf{F}_{\text{light}} = \frac{1}{2}\text{Re}[(\nabla\mathbf{E}^*)\cdot\mathbf{p}] + \frac{1}{2}\text{Re}[(\nabla\mathbf{H}^*)\cdot\mu_0\mathbf{m}] - \frac{k_0^4 c\mu_0}{12\pi}\text{Re}[\mathbf{p}\times\mathbf{m}^*], \tag{4}$$

where $\mathbf{p} = \epsilon_0\alpha_e\mathbf{E}$ is the electric dipole moment, $\mathbf{m} = \alpha_m\mathbf{H}$ is the magnetic dipole moment, $\alpha_e = i6\pi a_1/k_0^3$ is the electric polarizability of a spherical particle, and $\alpha_m = i6\pi b_1/k_0^3$ is its magnetic polarizability. The coefficients a_1 and b_1 are the first-order Mie scattering coefficients [25]

$$a_\nu = \frac{n^2 j_\nu(nx)[xj_\nu(x)]' - \mu j_\nu(x)[nxj_\nu(nx)]'}{n^2 j_\nu(nx)\left[xh_\nu^{(1)}(x)\right]' - \mu h_\nu^{(1)}(x)[nxj_\nu(nx)]'}, \tag{5}$$

$$b_\nu = \frac{\mu j_\nu(nx)[xj_\nu(x)]' - j_\nu(x)[nxj_\nu(nx)]'}{\mu j_\nu(nx)\left[xh_\nu^{(1)}(x)\right]' - h_\nu^{(1)}(x)[nxj_\nu(nx)]'}, \tag{6}$$

where $x = k_0R$, $n = \sqrt{\epsilon\mu}$ is the particle's refractive index, j_ν and $h_\nu^{(1)}$ are the spherical Bessel and Hankel functions of order ν, and the prime means the derivative with respect to the argument (e.g., $[nxj_\nu(nx)]' = d[nxj_\nu(nx)]/d(nx)$).

The force that a tractor beam exerts on a particle is found by inserting the electric and magnetic fields given by Eqs. (1) and (2) into (4). Near the beam axis ($k_0\rho \ll 1$), the expressions simplify and can be written as $\mathbf{F}_{\text{light}} = F_z\hat{\mathbf{z}} + F_\rho\hat{\boldsymbol{\rho}} + F_\phi\hat{\boldsymbol{\phi}}$, where

$$F_z^{\text{lin}} = F_z^{\text{circ}} = \frac{E_0^2\epsilon_0 k_0(\beta+1)^2}{4q^2} \times\left(\beta\text{Im}(\alpha_e+\alpha_m) - \frac{k^3}{6\pi}\text{Re}(\alpha_e\alpha_m^*)\right), \tag{7}$$

$$F_\phi^{\text{lin}} = \sin(2\phi)\frac{E_0^2\epsilon_0 k_0^2\rho}{8} \times\left(\frac{3q^2}{2}\text{Re}(\alpha_m-\alpha_e) - \frac{k^3(\beta+1)}{3\pi}\text{Im}(\alpha_e\alpha_m^*)\right), \tag{8}$$

$$F_\phi^{\text{circ}} = \frac{E_0^2\epsilon_0 k_0^2\rho}{8} \times\left(q^2\text{Im}(\alpha_e+\alpha_m) - \frac{k^3(\beta+1)}{3\pi}\text{Re}(\alpha_e\alpha_m^*)\right), \tag{9}$$

$$F_\rho^{\text{circ}} = -\frac{E_0^2\epsilon_0 k_0^2\beta(\beta+1)\text{Re}(\alpha_e+\alpha_m)\rho}{4}, \tag{10}$$

$$F_\rho^{\text{lin}} = F_\rho^{\text{circ}} + F_\phi^{\text{lin}}. \tag{11}$$

The superscripts *lin* and *circ* denote the force exerted by the linearly and circularly polarized tractor beams, respectively. It can be seen that the $\hat{\mathbf{z}}$-directed pulling force is identical for the two beams. In addition, both beams exert an inwardly directed gradient force. However, the circularly polarized tractor beam

contains an additional, nonconservative $\hat{\boldsymbol{\phi}}$-directed force, which makes this beam unstable without sufficient damping. In contrast, the $\hat{\boldsymbol{\phi}}$-directed force for the linearly polarized beam is multiplied by $\sin(2\phi)$, which reverses its sign depending upon the quadrant of the particle. The transverse force exerted by the linearly polarized tractor beam is conservative. This fact is most clearly identified by noting that near the beam axis, the transverse potential given by $-\nabla U = F_\rho^{\text{lin}}\hat{\boldsymbol{\rho}} + F_\phi^{\text{lin}}\hat{\boldsymbol{\phi}}$ can be written as

$$U = \epsilon_0 E_0^2 (k_0\rho)^2 \left[\left(\frac{\beta(\beta+1)}{8} \text{Re}(\alpha_e + \alpha_m) \right) - \cos(2\phi) \left(\frac{3q^2}{32} \text{Re}(\alpha_e - \alpha_m) + \frac{k_0^3(\beta+1)}{48\pi} \text{Im}(\alpha_e \alpha_m^*) \right) \right]. \quad (12)$$

A necessary condition for realizing an optical tractor beam is that α_e and α_m should be similar [8,9,20,21]. In this case, the potential is identical to a two-dimensional harmonic oscillator. In general, α_e is not exactly equal to α_m, which leads to an asymmetry in the potential proportional to the $\cos(2\phi)$ term.

IV. TRAJECTORY OF A PARTICLE PLACED IN A VACUUM

Let us consider some practical examples of linearly and circularly polarized tractor beams pulling a polystyrene sphere against the force of gravity, as shown in Fig. 1. For now, it is assumed that the particle is pulled through a vacuum (i.e., no ambient damping). The sphere is assumed to have a diameter equal to 750 nm and relative permittivity $\epsilon_r = 2.4$ at the operating wavelength 1.5 μm. The tractor beams have $E_0 = 2.5 \times 10^5$ V/m and $q = 0.94$, which correspond to a cone angle $\alpha = 70^\circ$. The total force acting on the particle is given by $\mathbf{F} = \mathbf{F}_{\text{light}} + g m_p \hat{\mathbf{z}} = m_p d\mathbf{v}/dt$, where $g = 9.8\,\text{m/s}^2$ is the gravitational constant and $m_p = 2.32 \times 10^{-16}$ kg is the mass of the particle.

The trajectory of the polystyrene particle is numerically solved by integrating Newton's equation using a Runge-Kutta method provided by MATLAB. Figure 2(a) shows the trajectory of the particle in the transverse plane (xy plane) when illuminated with a circularly polarized tractor beam. The particle is initially located at $(k_0x, k_0y) = (0.3, 0.3)$ with 0 velocity. It can be seen that the particle is initially pulled towards the center, but a $\hat{\boldsymbol{\phi}}$-directed force is also present, which drives the particle away from the center as time evolves. Eventually, this force causes the particle to run away from the beam axis. The particle's longitudinal position (z) is shown in Fig. 2(b). When the particle is located away from the beam axis, it is pushed rather than pulled by the source.

The trajectory of the particle when pulled by a linearly polarized tractor beam is shown in Fig. 2(c). The particle oscillates around the beam axis where the pulling force is maximal, but its distance from the center never exceeds the starting value. Figure 2(b) shows that the particle continuously accelerates towards the source ($-\hat{\mathbf{z}}$). Since the linearly polarized tractor beam exerts a conservative transverse force on the particle, a two-dimensional potential well can be defined and is plotted in Fig. 2(d). The asymmetry of the well is due to the fact that $\alpha_e \neq \alpha_m$ for the polystyrene sphere under consideration. This

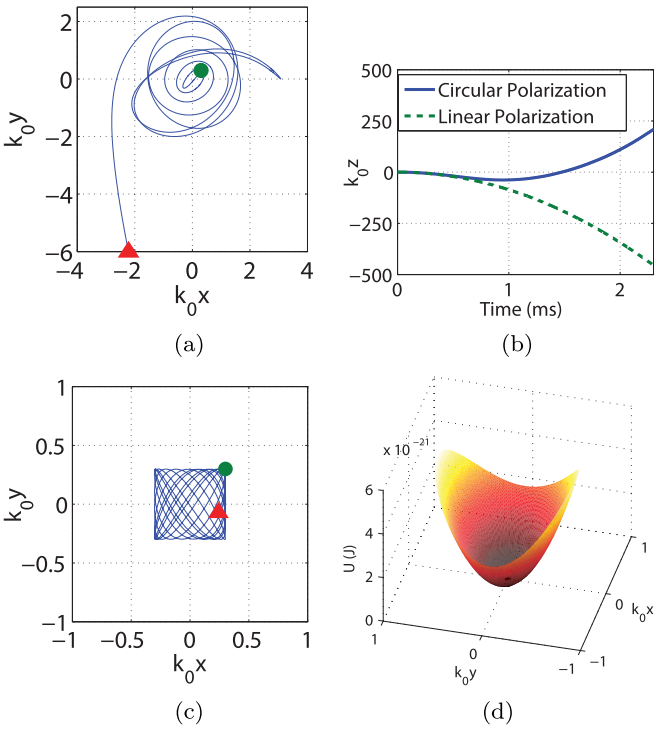

FIG. 2. (Color online) Trajectory of a 750-nm diameter polystyrene sphere when illuminated with circularly and linearly polarized tractor beams with $E_0 = 2.5 \times 10^5$ V/m and $q = 0.94$. At $t = 0$, the particle (denoted as a green circle) has 0 initial velocity and is located at $(k_0x, k_0y) = (0.3, 0.3)$. The particle's transverse position after 2.3 ms is indicated by a red triangle. (a) Transverse trajectory of the polystyrene sphere when illuminated with a circularly polarized tractor beam. After 2.3 ms, the particle is no longer confined near the beam axis. (b) Longitudinal position (z) of the particle as a function of time for the linearly and circularly polarized tractor beams. Only the linearly polarized tractor beam provides a stable pulling force. (c) Transverse trajectory of the polystyrene sphere when illuminated with a linearly polarized tractor beam. The particle is trapped near the beam axis where the pulling force is greatest. (d) Harmonic potential in the transverse plane that confines the polystyrene sphere to the axis of the linearly polarized tractor beam.

asymmetric potential causes the particle to map out the square shape shown in Fig. 2(c) as time progresses. No potential can be defined for the circularly polarized tractor beam since it exerts a nonconservative force on the particle.

V. TRAJECTORY OF A PARTICLE PLACED IN AIR

Let us now consider pulling the same particle through air, rather than a vacuum, which introduces viscous damping. The total force acting on the particle is now given by $\mathbf{F} = \mathbf{F}_{\text{light}} - \gamma\mathbf{v} + g m_p \hat{\mathbf{z}} = m_p d\mathbf{v}/dt$. The ambient damping constant of air is given by $\gamma = 6\pi\mu R = 1.3 \times 10^{-10}$ kg/s, where $\mu = 1.84 \times 10^{-5}$ kg/(m · s) is the dynamic viscosity of dry air at room temperature, and $R = 375$ nm is the radius of the polystyrene sphere.

It was noted several times that "sufficient damping" is required for the circularly polarized tractor beam to stably pull dielectric particles. This statement can be quantified,

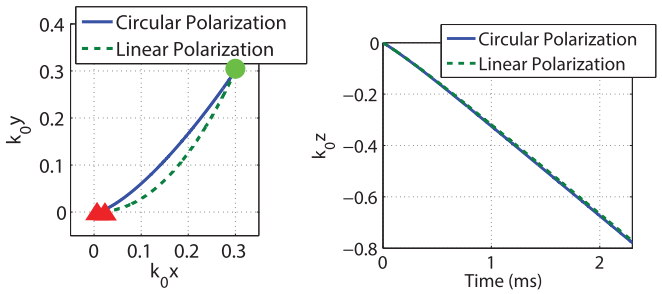

FIG. 3. (Color online) Trajectory of a 750-nm diameter polystyrene sphere when illuminated with circularly and linearly polarized tractor beams with $E_0 = 2.5 \times 10^5$ V/m and $q = 0.94$. At $t = 0$, the particle (denoted as a green circle) has 0 initial velocity and is located at $(k_0x, k_0y) = (0.3, 0.3)$. The particle's transverse position after 2.3 ms is indicated by a red triangle. (a) Transverse trajectory of the polystyrene sphere. (b) Longitudinal position (z) of the particle as a function of time.

and a detailed analysis was provided in Ref. [19]. In short, the transverse force on the particle can be written as $\mathbf{f} = \mathbf{f}_t + \mathbf{f}_d$, where $\mathbf{f}_t$ is the transverse optical force and $\mathbf{f}_d$ is the frictional force due to ambient damping. The transverse force can be written as $\mathbf{f} = \hat{\mathbf{K}}\Delta\boldsymbol{\rho} - \gamma d\Delta\boldsymbol{\rho}/dt$, where $\Delta\boldsymbol{\rho}$ is the displacement of the particle from the beam axis, γ is the ambient damping constant, and $\hat{\mathbf{K}}$ is a 2×2 matrix of the form

$$\hat{\mathbf{K}} = \begin{pmatrix} k_{11} & k_{12} \\ k_{21} & k_{22} \end{pmatrix}. \tag{13}$$

When the diagonal elements k_{11} and k_{22} are negative, they correspond to $\hat{\boldsymbol{\rho}}$-directed restoring forces. The off-diagonal elements k_{12} and k_{21} correspond to $\hat{\boldsymbol{\phi}}$-directed forces that rotate the particle around the beam axis. Only when the ambient damping sufficiently dissipates the rotational energy of the particle will the situation be stable. Due to the cylindrical symmetry of the circularly polarized tractor beam $k_{11} = k_{22}$ and $k_{12} = -k_{21}$. By analyzing the eigenvalues of Eq. (13), it can be shown that there is a critical damping constant that is required to confine the particle to the beam axis [19]

$$\gamma_{\text{critical}} = \sqrt{m_p}\frac{|k_{12}|}{\sqrt{|k_{11}|}}. \tag{14}$$

Combining this result with the optical forces acting on a small particle in Eqs. (9) and (10), the critical damping constant can be written in closed form

$$\gamma_{\text{critical}} = E_0\sqrt{m_p\epsilon_0} \times \frac{\left|q^2k_0\text{Im}(\alpha_e + \alpha_m) - \frac{k_0^4}{3\pi}(\beta+1)\text{Re}(\alpha_e\alpha_m^*)\right|}{4\sqrt{\beta(\beta+1)}\,|\text{Re}(\alpha_e + \alpha_m)|}. \tag{15}$$

Only when $\gamma > \gamma_{\text{critical}}$ will the particle be trapped along the circularly polarized tractor beam axis.

When $E_0 = 2.5 \times 10^5$ V/m and $q = 0.94$, the damping constant is $\gamma = 94.0\gamma_{\text{critical}}$. The large damping constant means that the circularly polarized beam is stable in this example. Figure 3 shows the trajectory of the particle when illuminated with circularly and linearly polarized tractor beams of a fixed

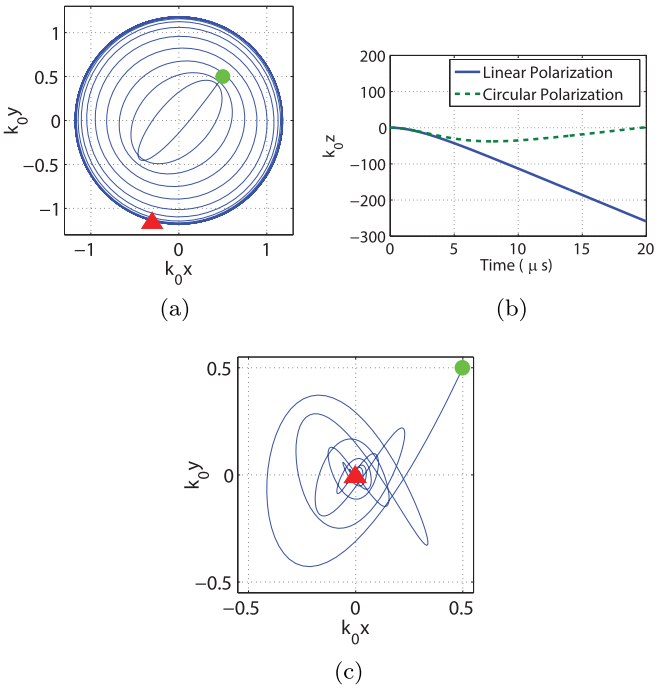

FIG. 4. (Color online) Trajectory of a 750-nm diameter polystyrene sphere when illuminated with circularly and linearly polarized tractor beams with $E_0 = 4.65 \times 10^7$ V/m and $q = 0.94$. At $t = 0$, the particle (denoted as a green circle) has 0 initial velocity and is located at $(k_0x, k_0y) = (0.5, 0.5)$. The particle's transverse position after 20 μs is indicated by a red triangle. (a) Transverse trajectory of the polystyrene sphere in air when illuminated with a circularly polarized tractor beam. Within 20 μs, the particle reaches equilibrium in a circular orbit at $k_0\rho = 1.18$. (b) Longitudinal position (z) of the particle as a function of time when the particle is in air and a vacuum, for linearly and circularly polarized tractor beams. Only the linearly polarized tractor beam provides a stable pulling force. (c) Transverse trajectory of the polystyrene sphere in air when illuminated with a linearly polarized tractor beam. Within 20 μs, the particle is trapped along the beam axis where the pulling force is greatest.

frequency. It can be seen that when the particle is initially located at $(k_0x, k_0y) = (0.3, 0.3)$, the gradient force moves the particle towards the beam axis, and the scattering force pulls the particle towards the source. By comparing the final position of the particle in Figs. 2(b) and in 3(b), it is clear that the particle is pulled much more slowly when it is surround by air rather than a vacuum.

It is also interesting to consider the case of pulling the particle through air by a tractor beam with much higher field intensity. If E_0 is increased from 2.5×10^5 V/m to 4.65×10^7 V/m, the air resistance is insufficient to stabilize the circularly polarized tractor beam ($\gamma = 0.51\gamma_{\text{critical}}$), as shown in Fig. 4(a). It can be seen that the particle is initially pulled towards the center, but a $\hat{\boldsymbol{\phi}}$-directed force is also present, which pushes the particle away from the center as time evolves. Eventually, the particle reaches equilibrium when the $\hat{\boldsymbol{\phi}}$-directed force, inwardly directed force, and the viscous damping balance each other. However, this steady-state location is away from the beam axis, where the longitudinal force pushes the particle away from the source rather than pulling

it in. This is verified in Fig. 4(b), which plots the particle's longitudinal position (z).

The trajectory of the particle when pulled through air by a linearly polarized beam is shown in Fig. 4(c). The particle initially oscillates around the beam axis, but then reaches a stable position at $\rho = 0$, where the pulling force is maximal. Figure 4(b) shows that the particle accelerates towards the source ($-\hat{\mathbf{z}}$) until it reaches a terminal velocity $v = 3.5$ m/s.

VI. GENERATING TRACTOR BEAMS WITH METASURFACES

Next, a simple method of generating these beams is introduced. Away from the beam axis ($k_0\rho \gg 1$), the linearly polarized tractor beam given by Eq. (1) can be written as a sum of TM and TE polarizations

$$\lim_{k_0\rho\gg 1} \mathbf{E} = \frac{iE_0 e^{i\beta k_0 z}}{q\sqrt{\pi k_0 q\rho}}((\hat{\mathbf{x}}\cdot\hat{\boldsymbol{\rho}})\mathbf{E}_{\mathrm{TM}} + (\hat{\mathbf{x}}\cdot\hat{\boldsymbol{\phi}})\mathbf{E}_{\mathrm{TE}}), \tag{16}$$

where

$$\mathbf{E}_{\mathrm{TM}} = (q\hat{\mathbf{z}} - \beta\hat{\boldsymbol{\rho}})e^{iqk_0\rho'} + (q\hat{\mathbf{z}} + \beta\hat{\boldsymbol{\rho}})e^{-iqk_0\rho'}, \tag{17}$$

$$\mathbf{E}_{\mathrm{TE}} = \hat{\boldsymbol{\phi}}(e^{iqk_0\rho'} - e^{-iqk_0\rho'}), \tag{18}$$

and $\rho' = \rho + \pi/(4qk_0)$. It can be seen from Eqs. (17) and (18) that the tractor beam is composed of equal amplitude, inwardly and outwardly propagating plane waves. It should be noted that the circularly polarized Gaussian beam is of the same form as Eqs. (16) to (18), but with $\hat{\mathbf{x}}$ replaced by $(\hat{\mathbf{x}} + i\hat{\mathbf{y}})/\sqrt{2}$.

There are several methods by which this interference pattern can be generated. One method of exactly generating the desired interference pattern is by illuminating a radially symmetric beam splitter with a normally incident, $\hat{\mathbf{x}}$-polarized plane wave. The incident $\hat{\mathbf{x}}$-polarized field can be broken up into $\hat{\boldsymbol{\rho}}$ and $\hat{\boldsymbol{\phi}}$ polarizations proportional to $\hat{\mathbf{x}}\cdot\hat{\boldsymbol{\rho}}$ and $\hat{\mathbf{x}}\cdot\hat{\boldsymbol{\phi}}$, as in Eq. (16). The $\hat{\boldsymbol{\rho}}$ component is representative of a TM-polarized wave and the $\hat{\boldsymbol{\phi}}$ component of a TE-polarized wave. The radially symmetric beam splitter then produces equal amplitude to inwardly and outwardly propagating TM- and TE-polarized plane waves that are given by Eqs. (17) and (18).

This situation is well approximated by illuminating the dielectric metasurface shown in Fig. 5 with a linearly polarized Gaussian beam [26]. Metasurfaces are ideal candidates for generating arbitrary beams since they are compact and have

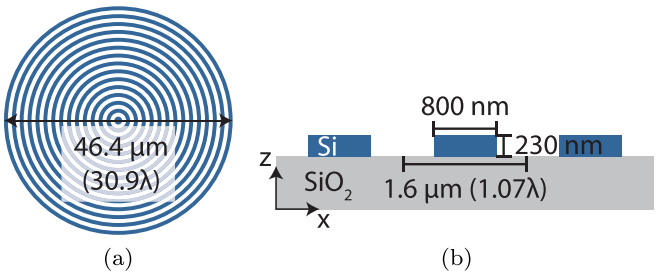

FIG. 5. (Color online) (a) Top view of the designed metasurface that converts a normally incident Gaussian beam into a linearly polarized tractor beam. The metasurface acts as a radially symmetric beam splitter. (b) Side view of the cross section of the metasurface.

demonstrated extreme control of a wave-front's amplitude, phase, and polarization [27–34]. Dielectric metasurfaces are particularly attractive since they are low loss and can handle high power [35–38]. The designed metasurface consists of a Si bullseye pattern on a bulk SiO_2 substrate. The inspiration for this geometry is derived from the extensive literature on binary phase gratings, which are commonly employed for interfering plane waves due to their simple design and fabrication processes [39–41]. The period of the grating determines the angles at which light will be transmitted, and the thickness of the Si determines the efficiency. When the duty cycle of Si is 50% and its thickness is roughly $\lambda_0/[2(n_{\mathrm{Si}} - 1)]$, the metasurface acts as an efficient beam splitter.

Binary phase gratings are commonly analyzed using scalar diffraction theory. However, this metasurface operates in a region where scalar diffraction theory is no longer valid due to the extreme (nonparaxial) cone angle and the high index of refraction of Si [42]. Therefore, the thickness of the Si is optimized using full wave simulations of a one-dimensional grating. The SiO_2 substrate is modeled as a lossless, infinite half space with an index of refraction of $n_{\mathrm{SiO_2}} = 1.54$ at the wavelength of 1.5 μm. The index of refraction of the Si is $n_{\mathrm{Si}} = 3.46$. When the Si is 230 nm thick, 60% of the incident power is split to the angles $\pm 70^\circ$ from normal, for both TM and TE polarizations. The primary sources of loss are reflection and transmission into the normal direction.

There are many alternative designs that could also be utilized. For example, the v-antenna array reported in Refs. [27,28] could be used to generate the desired transmitted phase profile given by Eqs. (16) to (18). In this case only the cross-polarized radiation would refocus into the tractor beam, which does limit the efficiency. The limited efficiency of single layer v-antenna designs can be significantly improved by cascading multiple patterned plasmonic sheets [31]. Refractory materials such as TiN may prove particularly useful for these devices since they can withstand high power levels [34].

Axicon lenses could also be utilized for generating tractor beams. These lenses are attractive because they are commercially available, and are commonly employed for generating Bessel beams. However, previously reported axicon lenses generated relatively small cone angles that are far too paraxial to produce a pulling force. It can be shown using geometrical optics that the axicon should be constructed from a material with large index of refraction to generate a tractor beam. For example, the index of the axicon lens must be at least $n = 2.924$ to realize a tractor beam with cone angle $\alpha = 70^\circ$. Otherwise the incident beam will be totally internally reflected. Alternatively, systems containing multiple, lower index axicon lenses could be used [43]. However, these systems suffer from increased complexity and size.

VII. SIMULATIONS

The metasurface shown in Fig. 5 is simulated using the full-wave solver ANSYS HFSS. The metasurface is illuminated with a normally incident Gaussian beam at a wavelength $\lambda_0 = 1.5$ μm. The beam waist radius is 20 μm and peak amplitude is $E = 3.4 \times 10^4$ V/m, which corresponds to an incident power of 1 mW. The transmitted beam contains the minimum power level that can pull a 750-nm polystyrene sphere against

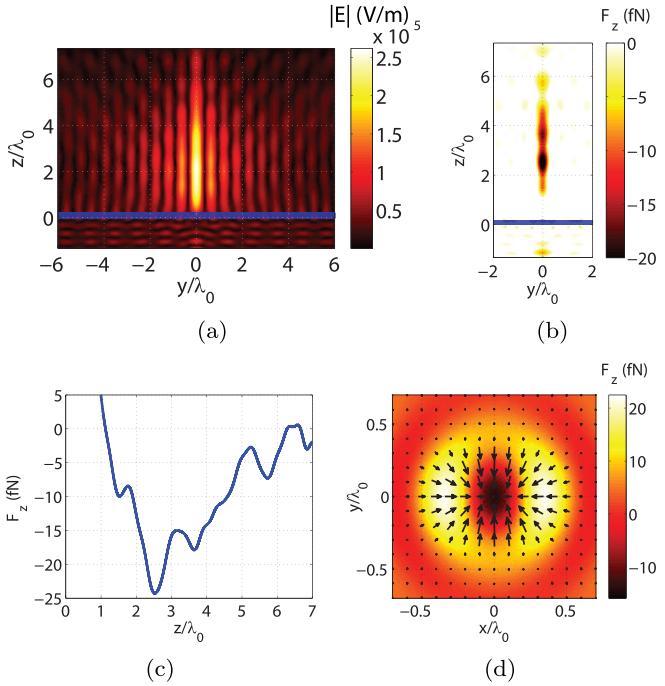

FIG. 6. (Color online) Simulated performance of the metasurface shown in Fig. 5. The metasurface is illuminated with an $\hat{\mathbf{x}}$-polarized, normally incident Gaussian beam with peak amplitude of $E = 3.4 \times 10^4$ V/m and wavelength $\lambda_0 = 1.5$ μm. The incident beam waist radius is $w_0 = 20$ μm. (a) Magnitude of the electric field along the yz plane. (b) Longitudinally directed force (F_z) exerted on a 750-nm diameter polystyrene sphere near the beam axis. Negative values correspond to a pulling force. (c) Profile of F_z along the beam axis. (d) Force field in the transverse plane $z = 3.15\lambda_0$. Color corresponds to $\hat{\mathbf{z}}$-directed force, while the arrows correspond to the transverse force field. It can be seen that the beam provides a stabilizing force towards its axis.

the force of gravity (2.3 fN) over its nondiffracting range ($z < \beta w_0$). Figure 6(a) plots the magnitude of the electric field in the yz plane. The high intensity line focus of the Bessel beam can be seen in the center. Using Eq. (4), the optical forces exerted on the polystrene sphere as a function of its position are numerically calculated from the simulated fields. Figures 6(b) and 6(c) plot the $\hat{\mathbf{z}}$-directed force in the yz plane and along the beam axis, respectively. It can be seen that the force is below -2.3 fN over a distance of $5\lambda_0$, which corresponds to the nondiffracting range of the beam. The beam stability is also verified by noting the transverse force field shown in Fig. 6(d).

From a practical perspective, the distance that a particle can be pulled scales linearly with the diameter of the metasurface and the incident Gaussian beam waist. Here, the diameter is limited to $30.9\lambda_0$ due to the computational resources available for simulating the entire structure using a full-wave solver. The transmitted beam more closely approximates an ideal tractor beam when the diameters of the metasurface and Gaussian beam are increased. Thus, these results should be viewed as a worst case scenario for larger metasurfaces. It is also important to note that the pulling distance scales as the square root of the incident power. For example, the same polystyrene particle could be pulled a distance exceeding $160\lambda_0$ if the metasurface diameter is increased to $980\lambda_0$ and the incident power is increased to 1 W.

VIII. SUMMARY

A straightforward method of stably pulling dielectric microparticles towards a source, independent of ambient conditions, is reported. In the future, the metasurface could be designed to compensate for truncation effects of tractor beams with finite size [44,45]. This would allow for a uniform pulling force along the beam axis. Alternatively, similar metasurface designs could be used to generate other highly structured optical modes, such as soleniod beams that pull microparticles along helical paths [11]. In addition, the metasurface could exhibit an anisotropic or bianisotropic response to provide micromanipulation control through polarization adjustment [33,46]. For example, it should be possible to control the degree at which microparticles are pushed or pulled by simply changing the polarization of the incident Gaussian beam [12,13]. This would allow for the arbitrary manipulation and sorting of small particles with a single beam. Furthermore, these beams may prove particularly useful for exploring new physical phenomena since they can stably pull particles through a vacuum [47,48].

ACKNOWLEDGMENTS

This work was supported by the NSF Materials Research Science and Engineering Center (MRSEC) Program No. DMR 1120923 and a Presidential Early Career Award for Scientists and Engineers FA9550-09-1-0696.

[1] Arthur Ashkin, Optical trapping and manipulation of neutral particles using lasers, Proc. Nat. Acad. Sci. **94**, 4853 (1997).
[2] Onofrio M. Maragò, Philip H. Jones, Pietro G Gucciardi, Giovanni Volpe, and Andrea C. Ferrari, Optical trapping and manipulation of nanostructures, Nat. Nanotechnol. **8**, 807 (2013).
[3] Arthur Ashkin, J. M. Dziedzic, and T. Yamane, Optical trapping and manipulation of single cells using infrared laser beams, Nature (London) **330**, 769 (1987).
[4] Arthur Ashkin and J. M. Dziedzic, Optical trapping and manipulation of viruses and bacteria, Science **235**, 1517 (1987).
[5] Yuanjie Pang, Hanna Song, Jin H. Kim, Ximiao Hou, and Wei Cheng, Optical trapping of individual human immunodeficiency viruses in culture fluid reveals heterogeneity with single-molecule resolution, Nat. Nanotechnol. **9**, 624 (2014).
[6] J. Arlt, V. Garces-Chavez, W. Sibbett, and K. Dholakia, Optical micromanipulation using a Bessel light beam, Opt. Commun. **197**, 239 (2001).
[7] Philip L. Marston, Axial radiation force of a Bessel beam on a sphere and direction reversal of the force, J. Acoust. Soc. Am. **120**, 3518 (2006).
[8] Jun Chen, Jack Ng, Zhifang Lin, and C. T. Chan, Optical pulling force, Nat. Photon. **5**, 531 (2011).

[9] Andrey Novitsky, Cheng-Wei Qiu, and Haifeng Wang, Single gradientless light beam drags particles as tractor beams, Phys. Rev. Lett. **107**, 203601 (2011).

[10] Aristide Dogariu, Sergey Sukhov, and José Sáenz, Optically induced 'negative forces', Nat. Photon. **7**, 24 (2013).

[11] Sang-Hyuk Lee, Yohai Roichman, and David G. Grier, Optical solenoid beams, Optics Exp. **18**, 6988 (2010).

[12] O. Brzobohatý, V. Karásek, M. Šiler, L. Chvátal, T. Čižmár, and P. Zemánek, Experimental demonstration of optical transport, sorting, and self-arrangement using a 'tractor beam', Nat. Photon. **7**, 123 (2013).

[13] Vladlen Shvedov, Arthur R. Davoyan, Cyril Hnatovsky, Nader Engheta, and Wieslaw Krolikowski, A long-range polarization-controlled optical tractor beam, Nat. Photon. **8**, 846 (2014).

[14] Christine E. M. Démoré, Patrick M. Dahl, Zhengyi Yang, Peter Glynne-Jones, Andreas Melzer, Sandy Cochran, Michael P. MacDonald, and Gabriel C. Spalding, Acoustic tractor beam, Phys. Rev. Lett. **112**, 174302 (2014).

[15] Horst Punzmann, Nicolas Francois, Hua Xia, Gregory Falkovich, and Michael Shats, Generation and reversal of surface flows by propagating waves, Nat. Phys. **10**, 658 (2014).

[16] Tomáš Čižmár, Veneranda Garcés-Chávez, Kishan Dholakia, and Pavel Zemánek, Optical conveyor belt for delivery of submicron objects, Appl. Phys. Lett. **86**, 174101 (2005).

[17] David B. Ruffner and David G. Grier, Optical conveyors: A class of active tractor beams, Phys. Rev. Lett. **109**, 163903 (2012).

[18] J. Durnin, Exact solutions for nondiffracting beams. I. The scalar theory, J. Opt. Soc. Am. A **4**, 651 (1987).

[19] Neng Wang, Jun Chen, Shiyang Liu, and Zhifang Lin, Dynamical and phase-diagram study on stable optical pulling force in Bessel beams, Phys. Rev. A **87**, 063812 (2013).

[20] Andrey Novitsky, Cheng-Wei Qiu, and Andrei Lavrinenko, Material-independent and size-independent tractor beams for dipole objects, Phys. Rev. Lett. **109**, 023902 (2012).

[21] Neng Wang, Wanli Lu, Jack Ng, and Zhifang Lin, Optimized optical tractor beam for core-shell nanoparticles, Optics Lett. **39**, 2399 (2014).

[22] Andrey V. Novitsky and Denis V. Novitsky, Negative propagation of vector Bessel beams, J. Opt. Soc. Am. A **24**, 2844 (2007).

[23] K. Volke-Sepulveda, V. Garcés-Chávez, S. Chávez-Cerda, J. Arlt, and K. Dholakia, Orbital angular momentum of a high-order Bessel light beam, J. Opt. B: Quantum Semiclassical Opt. **4**, S82 (2002).

[24] M. Nieto-Vesperinas, J. J. Sáenz, R. Gómez-Medina, and L. Chantada, Optical forces on small magnetodielectric particles, Optics Exp. **18**, 11428 (2010).

[25] Craig F. Bohren and Donald R. Huffman, *Absorption and Scattering of Light by Small Particles* (John Wiley & Sons, New York, 2008).

[26] F. Gori, G. Guattari, and C. Padovani, Bessel-Gauss beams, Opt. Commun. **64**, 491 (1987).

[27] N. Yu, P. Genevet, M. A. Kats, F. Aieta, J. P. Tetienne, F. Capasso, and Z. Gaburro, Light propagation with phase discontinuities: Generalized laws of reflection and refraction, Science **334**, 333 (2011).

[28] X. Ni, N. K. Emani, A. V. Kildishev, A. Boltasseva, and V. M. Shalaev, Broadband light bending with plasmonic nanoantennas, Science **335**, 427 (2012).

[29] Jiao Lin, Patrice Genevet, Mikhail A. Kats, Nicholas Antoniou, and Federico Capasso, Nanostructured holograms for broadband manipulation of vector beams, Nano Lett. **13**, 4269 (2013).

[30] C. Pfeiffer and A. Grbic, Metamaterial Huygens' surfaces: Tailoring wave fronts with reflectionless sheets, Phys. Rev. Lett. **110**, 197401 (2013).

[31] Carl Pfeiffer, Naresh Kumar Emani, Amr M. Shaltout, Alexandra Boltasseva, Vladimir M. Shalaev, and Anthony Grbic, Efficient light bending with isotropic metamaterial Huygens' surfaces, Nano Lett. **14**, 2491 (2014).

[32] Carl Pfeiffer and Anthony Grbic, Controlling vector Bessel beams with metasurfaces, Phys. Rev. Applied **2**, 044012 (2014).

[33] Carl Pfeiffer and Anthony Grbic, Bianisotropic metasurfaces for optimal polarization control: Analysis and synthesis, Phys. Rev. Applied **2**, 044011 (2014).

[34] Urcan Guler, Alexandra Boltasseva, and Vladimir M. Shalaev, Refractory plasmonics, Science **344**, 263 (2014).

[35] Zeev Bomzon, Gabriel Biener, Vladimir Kleiner, and Erez Hasman, Radially and azimuthally polarized beams generated by space-variant dielectric subwavelength gratings, Optics Lett. **27**, 285 (2002).

[36] Dianmin Lin, Pengyu Fan, Erez Hasman, and Mark L. Brongersma, Dielectric gradient metasurface optical elements, Science **345**, 298 (2014).

[37] Chihhui Wu, Nihal Arju, Glen Kelp, Jonathan A. Fan, Jason Dominguez, Edward Gonzales, Emanuel Tutuc, Igal Brener, and Gennady Shvets, Spectrally selective chiral silicon metasurfaces based on infrared Fano resonances, Nat. Commun. **5**, 3892 (2014).

[38] Annett B. Klemm, Daan Stellinga, Emiliano R. Martins, Liam Lewis, Guillaume Huyet, Liam O'Faolain, and Thomas F. Krauss, Experimental high numerical aperture focusing with high contrast gratings, Optics Lett. **38**, 3410 (2013).

[39] Wai-Hon Lee, High efficiency multiple beam gratings, Appl. Opt. **18**, 2152 (1979).

[40] Norbert Streibl, Beam shaping with optical array generators, J. Mod. Opt. **36**, 1559 (1989).

[41] Kasra Rastani, Abdellatif Marrakchi, Sarry F. Habiby, William M. Hubbard, Harold Gilchrist, and Robert E. Nahory, Binary phase Fresnel lenses for generation of two-dimensional beam arrays, Appl. Opt. **30**, 1347 (1991).

[42] Xufeng Jing and Yunxia Jin, Transmittance analysis of diffraction phase grating, Appl. Optics **50**, C11 (2011).

[43] Niklas Weber, Dominik Spether, Andreas Seifert, and Hans Zappe, Highly compact imaging using Bessel beams generated by ultraminiaturized multi-micro-axicon systems, J. Opt. Soc. Am. A **29**, 808 (2012).

[44] Tomáš Čižmár and Kishan Dholakia, Tunable Bessel light modes: Engineering the axial propagation, Optics Exp. **17**, 15558 (2009).

[45] Charles G. Durfee, John Gemmer, and Jerome V. Moloney, Phase-only shaping algorithm for Gaussian-apodized Bessel beams, Optics Exp. **21**, 15777 (2013).

[46] Carl Pfeiffer, Cheng Zhang, Vishva Ray, L. Jay Guo, and Anthony Grbic, High performance bianisotropic metasurfaces: Asymmetric transmission of light, Phys. Rev. Lett. **113**, 023902 (2014).

[47] Tongcang Li, Simon Kheifets, and Mark G. Raizen, Millikelvin cooling of an optically trapped microsphere in vacuum, Nat. Phys. **7**, 527 (2011).

[48] Yoshihiko Arita, Michael Mazilu, and Kishan Dholakia, Laser-induced rotation and cooling of a trapped microgyroscope in vacuum, Nat. Commun. **4**, 2374 (2013).